The nature and role of trap states in a dendrimer-based organic field-effect transistor explosive sensor

Guoqiang Tang, Simon S. Y. Chen, Kwan H. Lee, Almantas Pivrikas, Muhsen Aljada, Paul L. Burn, Paul Meredith, and Paul E. Shaw

Citation: Applied Physics Letters **102**, 243301 (2013); doi: 10.1063/1.4810914
View online: http://dx.doi.org/10.1063/1.4810914
View Table of Contents: http://scitation.aip.org/content/aip/journal/apl/102/24?ver=pdfcov
Published by the AIP Publishing

The nature and role of trap states in a dendrimer-based organic field-effect transistor explosive sensor

Guoqiang Tang, Simon S. Y. Chen, Kwan H. Lee, Almantas Pivrikas, Muhsen Aljada, Paul L. Burn,[a] Paul Meredith,[b] and Paul E. Shaw
Centre for Organic Photonics & Electronics, The University of Queensland, Brisbane 4072, Australia

(Received 28 March 2013; accepted 28 May 2013; published online 17 June 2013)

We report the fabrication and charge transport characterization of carbazole dendrimer-based organic field-effect transistors (OFETs) for the sensing of explosive vapors. After exposure to *para*-nitrotoluene (*p*NT) vapor, the OFET channel carrier mobility decreases due to trapping induced by the absorbed *p*NT. The influence of trap states on transport in devices before and after exposure to *p*NT vapor has been determined using temperature-dependent measurements of the field-effect mobility. These data clearly show that the absorption of *p*NT vapor into the dendrimer active layer results in the formation of additional trap states. Such states inhibit charge transport by decreasing the density of conducting states. © *2013 AIP Publishing LLC*. [http://dx.doi.org/10.1063/1.4810914]

Organic field-effect transistors (OFETs) are central component elements in next generation "plastic electronics." OFETs can be used in a diverse range of applications such as active matrix display backplanes,[1–3] radio frequency identification (RFID) transponders (tags),[4] complementary inverters,[5,6] and light-emitting field-effect transistors,[7–9] with their appeal due to a combination of features including mechanical flexibility, being light weight, and potentially having a low cost.[10] In the past decade, there have been a number of reports of OFET sensors being used to detect/monitor vapor phase targets such as nitrogen oxide[11,12] and solvent vapors.[13,14] In contrast, there have been only a small number of publications on OFETs developed for detecting biological nerve gas simulants[15] and explosives.[16,17] The majority of OFETs reported to date, particularly in sensor applications, have polymeric or small molecule organic semiconductor channels.[11,13–20] We have recently demonstrated sensing OFETs based upon a third class of materials—namely semiconducting dendrimers.[21] Dendrimers are branched macromolecules composed of a core, branching units and surface groups.[22] The properties of each element of the dendrimer can be independently tuned to control solubility, transport properties, molecular ordering, and structural compatibility with a sensing target. Solution processability simplifies device fabrication, and this is a core advantage of the carbazole dendrimer featured in this letter. Furthermore, the ability to precisely engineer the molecular structure and energetics makes them ideal platforms to create analyte-specific electrical, chemical, or photophysical sensing elements. We have previously reported a number of dendrimer families that are able to detect a range of explosive analytes.[23–25] These materials have been designed to sense via a photophysical mechanism whereby the target analyte interacts with and efficiently quenches the photoluminescence of the dendrimer through photo-induced electron transfer. For this mechanism to work, the dendrimer must have an excited state ionization potential I_p* more positive than the analyte ground state electron affinity E_A to enable electron transfer to occur, thus leading to a non-radiative decay pathway. Furthermore, the molecular structure of the sensing dendrimer can be engineered to promote binding of the analyte—the strength and nature of this binding dictates whether the quenching mechanism is static or collisional.

One dendrimer family of particular interest is based upon a spirobifluorene core, carbazole dendrons, and fluorenyl surface groups.[25] We have previously shown these materials to be photoluminescent in both solution and the solid-state, and to have a strong photophysical sensing response to a range of explosive analytes.[25] The first generation dendrimer (with a single branching point and denoted G1) is shown in Figure 1(a). In the solid-state, this material forms an amorphous thin film. Furthermore, we have shown that G1 has respectable charge transport in an OFET with an average hole mobility of 6.6×10^{-5} cm^2/Vs.[21,26] In addition, G1 has a strong affinity for explosive analytes and this coupled with its electrical performance means it is a natural candidate as an active sensing channel in an organic transistor. Based on this, we recently demonstrated that the source-drain (I_{ds}) current of an OFET with a G1 dendrimer channel was strongly modulated upon exposure to saturated *para*-nitrotoluene (*p*NT) vapor (a chemically similar compound to the explosive 2,4,6-trinitrotoluene (TNT)).[21] This modulation was caused by a dramatic decrease in the carrier mobility, and the effect was reversible upon heating. The device showed good reproducibility when the bias stress was significantly decreased by applying a pulsed gate voltage. In this communication we explore the mechanism responsible for this sensing behavior. We use temperature-dependent mobility measurements to probe the thermal activation of the trap states—both intrinsic to the dendrimer semiconductor, and those induced by the *p*NT. The results show that the decrease in source-drain current upon exposure to the analyte is due to the creation of hole-trap states, which suppress the majority carrier mobility. Such mechanistic understanding is crucial in designing selective sensing systems based upon the modulation of electrical properties in organic semiconductors.

[a]Electronic address: p.burn2@uq.edu.au
[b]Electronic address: meredith@physics.uq.edu.au

The top-contact, bottom-gate OFET devices (see Figure 1(b)) were prepared on silicon substrates with a 350 nm layer of thermally grown dioxide as the dielectric, the surface of which was passivated with *n*-octyltrichlorosilane (OTS).[26] A 20 mg/ml dendrimer solution in toluene was then spin-coated onto the substrates in a nitrogen atmosphere at 1500 rpm for 60 s to give a film approximately 100 nm thick. Lastly, interdigitated source and drain contacts comprised of 15 nm molybdenum (VI) oxide and 30 nm of gold were evaporated onto the dendrimer film. Devices with three different channel dimensions (W = 40 mm, L = 40 μm; W = 50 mm, L = 120 μm; W = 50 mm, L = 80 μm) were fabricated (W = width; L = length). The devices were aged in air in the dark for a minimum of 2 days before testing to enable them to equilibrate to the ambient atmospheric conditions. The OFET performance was characterized in the dark in air using an Agilent B1500A semiconductor analyzer. The transfer characteristics of the devices were subsequently measured under ambient conditions before *p*NT exposure, after a 1 min saturated *p*NT exposure, and after heating at 80 °C for 5 min. Exposure to *p*NT vapor was achieved by placing the device in a jar containing solid *p*NT covered with cotton wool for 1 min. The role of the cotton wool was to prevent direct contact between the solid *p*NT and the device and maintain a constant vapor pressure. Removal of the *p*NT from the devices was achieved by heating on a hotplate at 80 °C in air for 5 min. For the temperature-dependent field-effect measurements, the OFET devices were first mounted on a chip using silver paste to provide adhesion and good electrical and thermal contact. This chip was placed in a Janis SHZ-950 cryostat, which was then placed under vacuum and backfilled with helium three times. It should be noted that these conditions are not sufficient to completely remove the *p*NT absorbed by the dendrimer. The measurements were also obtained in a helium atmosphere. The temperature was controlled with a Lakeshore 340 system over the range of 240 K to 300 K.

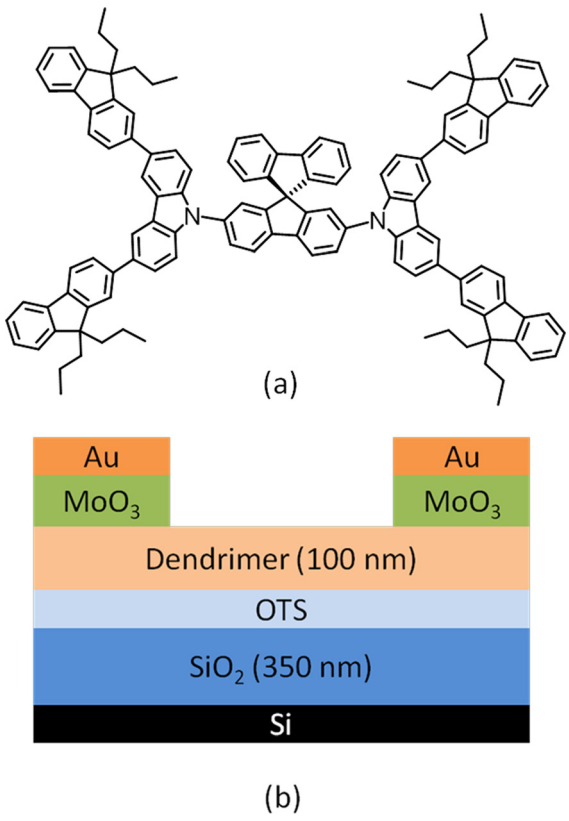

FIG. 1. (a) Molecular structure of G1. (b) Architecture of G1 active channel OFET.

Typical source-drain current-voltage (I_{ds}-V_{ds}) output characteristics for a G1 OFET tested in air are shown in Figure 2 (W:L = 50 mm:80 μm). The device displayed *p*-type behavior with clear linear and saturation regimes and an initial threshold voltage (V_{th}) of around -10 ± 3 V. The "air-aged" devices exhibited comparable carrier mobility and threshold voltages to freshly prepared devices measured under inert conditions.[26] Good air stability is highly desirable for any sensing technology to be used in the field.

Figure 3 shows the transfer characteristics of a W:L = 50 mm:80 μm OFET before and after 1 min exposure to saturated *p*NT vapor, and after the heat recovery process (80 °C, 5 min). In the limit that carrier mobility is independent of gate voltage, and neglecting short-channel effects, the saturation drain current $I_{ds,sat}$ of an OFET is given by[27,28]

$$I_{ds,\,sat}^{1/2} = \left(\frac{W}{2L} c\mu_{sat}\right)^{1/2} (V_g - V_{th}), \tag{1}$$

where c is the dielectric capacitance per unit area, μ_{sat} is the saturation mobility, and V_g and V_{th} are the gate and threshold voltages, respectively. Using Eq. (1), we can calculate the carrier mobility before and after *p*NT exposure and subsequent heat recovery. The threshold voltage was also obtained from the intercept of linear fits to the transfer characteristics.

When analyte molecules are absorbed, changes occur in μ_{sat} and V_{th}, noted as $\Delta\mu$ and ΔV_{th}, so that the saturation drain current $I_{sat(analyte)}$ of the OFET becomes

$$I_{sat(analyte)}{}^{1/2} = \left[\frac{W}{2L} c(\mu_{sat} + \Delta\mu)\right]^{1/2} \left[V_g - (V_{th} + \Delta V_{th})\right]. \tag{2}$$

Combining Eqs. (1) and (2), we can obtain the relationship between $I_{sat(analyte)}$ and I_{sat}, given by

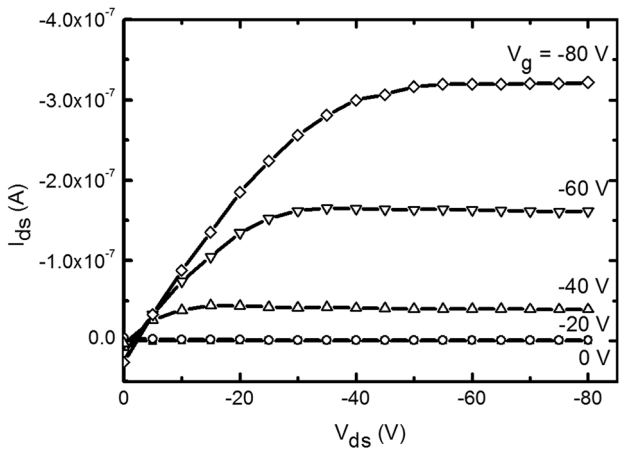

FIG. 2. Typical I_{ds}-V_{ds} output of a G1 OFET measured in air in the dark with V_{ds} sweeping from 10 V to −80 V and V_g sweeping from 10 V to −80 V.

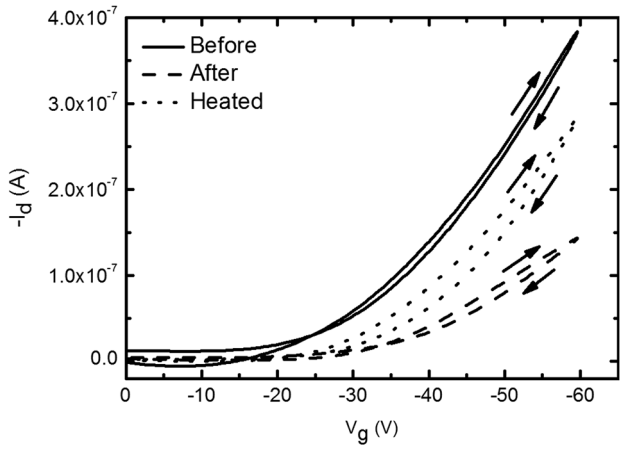

FIG. 3. Transfer characteristics of a G1 OFET (W:L = 50 mm:80 μm) in the saturation regime. Solid lines are transfer curves with the gate sweeping forward and backward before *p*NT exposure; dashed lines are that of the device after 1 min exposure to saturated *p*NT vapor; dotted lines are that of the device after 5 min heating at 80 °C.

$$\frac{I_{sat(analyte)}}{I_{sat}} = \left(1 + \frac{\Delta\mu}{\mu_{sat}}\right)\left[1 - \left(\frac{\Delta V_{th}}{V_g - V_{th}}\right)\right]^2. \quad (3)$$

This equation is only valid when $|\Delta V_{th}| < |V_g - V_{th}|$ and represents the gate voltage dependence of the sensor response. Based on the data in Figure 3, the calculated μ_{sat} decreases from $(5.7 \pm 0.1) \times 10^{-5}$ cm^2/Vs to $(3.5 \pm 0.1) \times 10^{-5}$ cm^2/Vs (~40% change) after a 1 min *p*NT vapor exposure. The V_{th} increased from -13 ± 0.6 V to -22 ± 1.8 V after exposure to *p*NT and a stronger hysteresis was observed. The calculated decrease of the saturation current (when $V_g = -60$ V) after *p*NT exposure is ~60%, which is consistent with the measured current decrease (~60%). The threshold voltage of the control device also shows a negative shift (voltage increase) from -7 ± 0.5 V to -14 ± 0.7 V after a 1 min air exposure but with no change in the carrier mobility $(4.2 \pm 0.1) \times 10^{-5}$ cm^2/Vs. The errors quoted were derived from the uncertainty in the linear fits to the transfer curves.

We have previously shown that heating a G1 device at 80 °C can overcome the binding between the dendrimer and the *p*NT, promoting the release of the *p*NT.[21] From the transfer outputs of the device in Figure 3, about 75% of the initial current was recovered after heating while the carrier mobility returned to $(5.6 \pm 0.1) \times 10^{-5}$ cm^2/Vs. This indicates that bias stress causes some carriers to remain in long-lived trap states[29] in the dendrimer channel,[30–32] a conclusion which is also supported by the irreversible change of both the threshold voltage (-19 V $\pm$ 1.1 V) and hysteresis behavior.

Carrier transport in amorphous organic semiconductors is mediated *via* thermally activated hopping.[33] Under such circumstances, the carrier mobility is strongly affected by the probability of a hopping transition—which in turn depends upon the local chemical potential landscape. Hence, it is plausible that the introduction of *p*NT into the G1 OFET creates energetically deep traps, which inhibit carrier hopping and decrease the channel mobility. To test this hypothesis and further elucidate the transport physics, we performed temperature-dependent carrier mobility measurements. Figure 4 shows the mobility of a G1 OFET (W = 50 mm; L = 120 μm) as a function of temperature for a device before and after exposure to

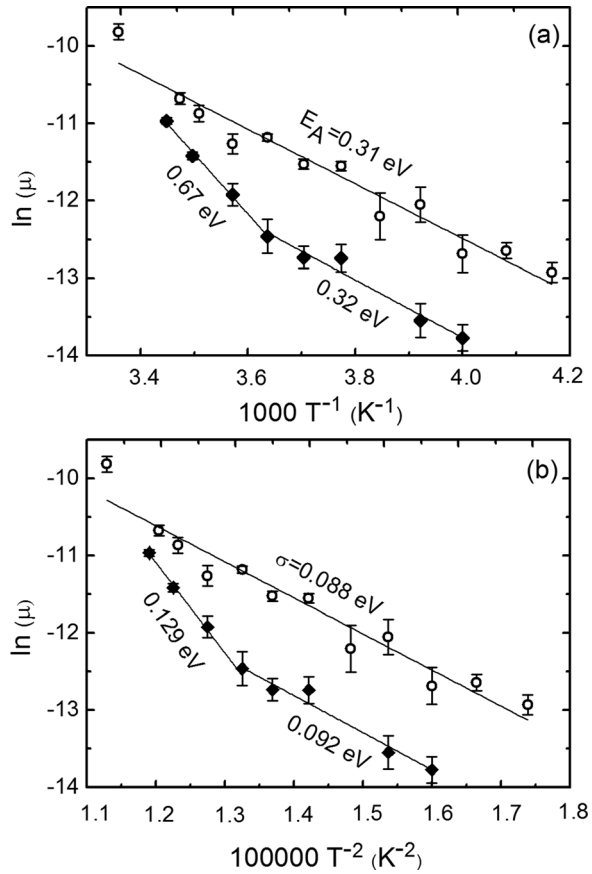

FIG. 4. Temperature dependence of the carrier mobility of a G1 OFET before (empty circles) and after exposure to saturated *p*NT vapor (filled diamonds). (a) Fits to Eq. (4) reveal the activation energy of different trap types; (b) fits to Eq. (5) reveal the overall width of the distribution of the states.

saturated *p*NT vapor for 1 min. While the non-exposed device shows a single temperature dependency as we would expect for a uniform distribution of trap states, after exposure to *p*NT there are two distinct regions indicative of two types of trap states.

The change in the charge carrier mobility with temperature can be described to first order by

$$\mu = \mu_0 \exp\left(-\frac{E_A}{K_B T}\right), \quad (4)$$

where μ is the carrier mobility, μ_0 is the mobility in the absence of energetic disorder, E_A is the activation energy, T is the temperature, and K_B is Boltzmann's constant.[34] Fits to the data for the non-exposed device with Eq. (4) (shown in Figure 4(a)) are consistent with "Arrhenius-like" behavior with an activation energy of 0.31 ± 0.04 eV for the cooling cycle and 0.29 ± 0.05 eV for the heating cycle (not shown). This is consistent with a single type (population) of hole-traps. Fits to the data for the device exposed to *p*NT give an activation energy of 0.32 ± 0.05 eV in the lower temperature region (240–275 K) and 0.67 ± 0.04 eV in the high temperature region (275–290 K). We can, therefore, identify both intrinsic trap states (~0.3 eV) and *p*NT-induced trap states (~0.7 eV). Measurements performed on devices with a different channel width and length ($W = 40$ mm, $L = 40$ μm) yielded similar activation energies of 0.33 ± 0.04 eV and 0.72 ± 0.03 eV, indicating that the traps are not related to the

channel dimensions but are a property of the active layer material. The errors quoted here were derived from the uncertainty in the linear fits.

To investigate the role of *p*NT-induced traps on charge transport in the dendrimer film, the data were fitted with a model for carrier mobility within a Gaussian density of states (DOS) as described by Bässler.[35,36] The Gaussian Disorder Model (GDM) has previously been successfully applied to explain the electric field and voltage dependence of transport in strongly disordered organic semiconductor films. The mobility within this framework can be expressed as

$$\mu = \mu_0 \exp\left[-\left(\frac{2\sigma}{3K_BT}\right)^2\right], \quad (5)$$

where σ is the Gaussian width of the electronic state distribution. It should be noted that an electrical field-related second exponential factor in both Eqs. (4) and (5) can be neglected due to the relatively low V_{ds} field (up to ~6000 V/cm). The data and the associated fits with Eq. (5) are shown in Figure 4(b). Prior to exposure to *p*NT the device displayed a linear dependence which yielded a single value of σ of 0.088 ± 0.003 eV. After exposure to *p*NT, the data show two regions of differing temperature dependence. This behaviour is not consistent with the Gaussian Disorder Model as expressed in Eq. (5) in which we would have expected a single Gaussian distribution representing energetic disorder, albeit broadened with respect to the non-exposed case. Hence, we hypothesize that two distinct conduction pathways exist within the channel of the exposed device: one where transport through the device is disrupted by the presence of *p*NT and one where it is not. At high *p*NT concentrations, the dendrimer film can swell causing disruption of the local order and changes to the global temperature dependence. In this current study, we did not observe film swelling and the device exposure area was limited—from this we conclude that the measurements were made in the low concentration limit. With this in mind, by fitting to the two regimes separately (i.e., the GDM over a very limited temperature regime), we obtained values for σ of 0.129 ± 0.004 eV in the high temperature region and 0.092 ± 0.003 eV in the low temperature region. The errors again were derived from the linear fits. In the low temperature region, the charge carriers trapped in intrinsic defect states can be activated, displaying a similar σ as prior to *p*NT exposure. In the high temperature region, the charge carriers trapped in both the intrinsic and *p*NT-induced trap states can be activated, displaying a broadened DOS and thus larger σ. Such broadening of the DOS could plausibly lead to a decrease of the density of conducting states and an increase in the density of lower energy tail states, resulting in an overall decrease of the mobility which is easily seen in Figure 4. Hence, the temperature-dependent measurements support the proposition that *p*NT absorption induces transport inhibiting deeper level trap states in the G1 dendrimer semiconducting channel.

In conclusion, we have investigated the interaction between nitroaromatic explosive vapors and the sensing channel of a dendrimer-based OFET. Transfer characteristic measurements showed a decrease in *p*-type carrier mobility primarily caused by absorption of *p*NT into the dendrimer semiconducting channel. Heating of the device resulted in the release of the *p*NT from the dendrimer and a restoration of the carrier mobility. The trap state energies in a device before and after exposure to *p*NT vapor were characterized with temperature-dependent measurements of the field-effect mobility. These showed that the absorption of *p*NT vapor resulted in the formation of additional higher energy (deeper) trap states, which inhibit hole transport by decreasing the population of conduction states. This additional insight can potentially be of great benefit in designing and characterizing OFETs intended for sensing applications.

P.M. and P.L.B. are supported by University of Queensland Vice Chancellor's Research Fellowships. G.T. was supported by an UQIPRS and SYC an Australian Postgraduate Award. P.E.S. and A.P. are the recipients of Australian Research Council Discovery Early Career Researcher Awards. The research was funded by the Australian Research Council under the Discovery Program (DP0986838). This work was performed in part at the Queensland node of the Australian National Fabrication Facility (ANFF-Q)—a company established under the National Collaborative Research Infrastructure Strategy to provide nano- and micro fabrication facilities for Australia's researchers.

[1]J. A. Rogers, Z. Bao, K. Baldwin, A. Dodabalapur, B. Crone, V. R. Raju, V. Kuck, H. Katz, K. Amundson, J. Ewing, and P. Drzaic, Proc. Natl. Acad. Sci. U.S.A. **98**, 4835 (2001).
[2]G. H. Gelinck, H. E. A. Huitema, E. Van Veenendaal, E. Cantatore, L. Schrijnemakers, J. B. P. H. Van der Putten, T. C. T. Geuns, M. Beenhakkers, J. B. Giesbers, B. H. Huisman, E. J. Meijer, E. M. Benito, F. J. Touwslager, A. W. Marsman, B. J. E. Van Rens, and D. M. De Leeuw, Nature Mater. **3**, 106 (2004).
[3]L. S. Zhou, A. Wanga, S. C. Wu, J. Sun, S. Park, and T. N. Jackson, Appl. Phys. Lett. **88**, 083502 (2006).
[4]P. F. Baude, D. A. Ender, M. A. Haase, T. W. Kelley, D. V. Muyres, and S. D. Theiss, Appl. Phys. Lett. **82**, 3964 (2003).
[5]H. Klauk, U. Zschieschang, J. Pflaum, and M. Halik, Nature **445**, 745 (2007).
[6]T. B. Singh, P. Senkarabacak, N. S. Sariciftci, A. Tanda, C. Lackner, R. Hagelauer, and G. Horowitz, Appl. Phys. Lett. **89**, 033512 (2006).
[7]J. Zaumseil, R. H. Friend, and H. Sirringhaus, Nature Mater. **5**, 69 (2006).
[8]E. B. Namdas, B. B. Y. Hsu, Z. H. Liu, S. C. Lo, P. L. Burn, and I. D. W. Samuel, Adv. Mater. **21**, 4957 (2009).
[9]J. H. Seo, E. B. Namdas, A. Gutacker, A. J. Heeger, and G. C. Bazan, Appl. Phys. Lett. **97**, 043303 (2010).
[10]T. Sekitani, U. Zschieschang, H. Klauk, and T. Someya, Nature Mater. **9**, 1015 (2010).
[11]F. Marinelli, A. Dell'Aquila, L. Torsi, J. Tey, G. P. Suranna, P. Mastrorilli, G. Romanazzi, C. F. Nobile, S. G. Mhaisalkar, N. Cioffi, and F. Palmisano, Sens. Actuators B **140**, 445 (2009).
[12]A. M. Andringa, J. R. Meijboom, E. C. P. Smits, S. G. J. Mathijssen, P. W. M. Blom, and D. M. de Leeuw, Adv. Funct. Mater. **21**, 100 (2011).
[13]A. Das, R. Dost, T. H. Richardson, M. Grell, D. C. Wedge, D. B. Kell, J. J. Morrison, and M. L. Turner, Sens. Actuators B **137**, 586 (2009).
[14]D. C. Wedge, A. Das, R. Dost, J. Kettle, M. B. Madec, J. J. Morrison, M. Grell, D. B. Kell, T. H. Richardson, S. Yeates, and M. L. Turner, Sens. Actuators B **143**, 365 (2009).
[15]T. Someya, A. Dodabalapur, J. Huang, K. C. See, and H. E. Katz, Adv. Mater. **22**, 3799 (2010).
[16]M. Erouel, K. Diallo, J. Tardy, P. Blanchard, J. Roncali, P. Frere, and N. Jaffrezic, Mater. Sci. Eng., C **28**, 965 (2008).
[17]J. Huang, T. J. Dawidczyk, B. J. Jung, J. Sun, A. F. Mason, and H. E. Katz, J. Mater. Chem. **20**, 2644 (2010).
[18]R. S. Dudhe, S. P. Tiwari, H. N. Raval, M. A. Khaderbad, R. Singh, J. Sinha, M. Yedukondalu, M. Ravikanth, A. Kumar, and V. R. Rao, Appl. Phys. Lett. **93**, 263306 (2008).
[19]A. Das, R. Dost, T. Richardson, M. Grell, J. J. Morrison, and M. L. Turner, Adv. Mater. **19**, 4018 (2007).

[20]B. Crone, A. Dodabalapur, A. Gelperin, L. Torsi, H. E. Katz, A. J. Lovinger, and Z. Bao, Appl. Phys. Lett. **78**, 2229 (2001).
[21]G. Tang, S. S. Y. Chen, M. Aljada, P. L. Burn, and P. Meredith, Org. Electron. **14**, 1255 (2013).
[22]K. A. Knights, S. G. Stevenson, C. P. Shipley, S.-C. Lo, S. Olsen, R. E. Harding, S. Gambino, P. L. Burn, and I. D. W. Samuel, J. Mater. Chem. **18**, 2121 (2008).
[23]H. Cavaye, P. E. Shaw, X. Wang, P. L. Burn, S.-C. Lo, and P. Meredith, Macromolecules **43**, 10253 (2010).
[24]A. J. Clulow, P. L. Burn, P. Meredith, and P. E. Shaw, J. Mater. Chem. **22**, 12507 (2012).
[25]G. Tang, S. S. Y. Chen, P. E. Shaw, K. Hegedus, X. Wang, P. L. Burn, and P. Meredith, Polym. Chem. **2**, 2360 (2011).
[26]K. Mutkins, S. S. Y. Chen, M. Aljada, B. J. Powell, S. Olsen, P. L. Burn, and P. Meredith, Proc. SPIE **8117**, 811704 (2011).
[27]G. Horowitz, Adv. Mater. **10**, 365 (1998).
[28]F. Garnier, G. Horowitz, X. Z. Peng, and D. Fichou, Synth. Met. **45**, 163 (1991).
[29]A. Salleo, F. Endicott, and R. A. Street, Appl. Phys. Lett. **86**, 263505 (2005).
[30]D. Knipp, R. A. Street, A. Volkel, and J. Ho, J. Appl. Phys. **93**, 347 (2003).
[31]A. Salleo and R. A. Street, J. Appl. Phys. **94**, 4231 (2003).
[32]R. A. Street, A. Salleo, and M. L. Chabinyc, Phys. Rev. B **68**, 085316 (2003).
[33]Z. Bao and J. Locklin, *Organic Field-Effect Transistors* (CRC Press, Taylor and Francis Group, 2007).
[34]W. D. Gill, J. Appl. Phys. **43**, 5033 (1972).
[35]H. Bässler, Philos. Mag. B **50**, 347 (1984).
[36]L. Pautmeier, R. Richert, and H. Bässler, Synth. Met. **37**, 271 (1990).